Attitude Determination for the NANOSTAR Project

Hugo Miguel Martins Marques
hugo.m.marques@tecnico.ulisboa.pt

Instituto Superior Técnico, Lisboa, Portugal

November 2019

Abstract

The Attitude Determination and Control System (ADCS) of a nanosatellite is a key subsystem to provide precise attitude knowledge and pointing for the on-board payload and necessary maneuvers. Its design has serious constraints in terms of mass, volume, size, cost and power. The main goal of this dissertation is to provide the NANOSTAR project with a grounded study in terms of attitude determination algorithms and sensors that can be employed in the missions designed under the scope of the project. For that, a simulation platform that realistically describes the nanosatellite environment, allowing orbit generation and propagation, as well as data creation to feed the ADCS was developed. Then, three representative attitude determination algorithms, namely the Quaternion Estimator (QUEST), the Multiplicative Extended Kalman Filter (MEKF), and a recently developed Globally Exponentially Stable Cascade Attitude Nonlinear Observer, were studied and implemented on the platform developed, using vector measurements provided by a star tracker, Sun sensor, magnetometer and rate gyroscope. Finally, the comparison of the three algorithms in terms of computational resources efficiency, steady-state performance and performance in the case of faults is done, using realistic simulation scenarios. The results obtained provide meaningful insight on the advantages, disadvantages, complexity, computational resources efficiency and performance of the three algorithms, providing the project with a grounded analysis that can be used for future decision making in terms of the ADCS design.

Keywords: Attitude Determination, Nanosatellite, Deterministic Methods, Kalman Filter, Nonlinear Observer

1. Introduction

1.1. Motivation and Goals

The trend in satellites, present in the last decades, to do more for less cost, having smaller, cheaper, faster and better space missions, has led to the decrease of spacecraft sizes, accompanied by strict mass, volume, power and cost constraints. The segment of nanosatellites is of particular interest, with the highlight going to the CubeSats. Nanosatellite missions objectives [2] range from technology demonstration and operational use, to university programs providing "hands-on" experience. The Attitude Determination and Control System (ADCS) is a key subsystem of a nanosatellite to provide precise pointing for the on-board payloads and maneuvers. Nowadays nanosatellites have its ADCS composed of miniaturized and novel precise attitude sensors and actuators and proper attitude determination algorithms and active control schemes.

The work done was under the scope of the NANOSTAR Project [14]. NANOSTAR is a collaborative project, funded by the Interreg Sudoe Programme through the European Regional Development Fund (ERDF), among universities, aerospace clusters and ESA Business Incubation Centers, from Southern Europe. The project aims at providing students with the experience of a real space engineering process that includes all stages, from conception and specifications, to design, assembly, integration, testing and documentation. The training on technology of nanosatellites is to be provided through several design, development and testing student challenges. To date, two nanosatellite space mission preliminary design challenges were launched, one that consists in a mission around the Moon, and the other around the Earth. The two missions referred need to guarantee the pointing of its payload, hence a detailed design and testing challenge for the ADCS of the two missions was recently launched. Therefore, this work proposes to: 1) Select a sensor suite adequate for both missions; 2) Create a reliable simulation platform that realistically simulates the spacecraft's environment, allowing orbit generation and propagation, as well as data creation to feed the ADCS; 3) Study, adapt and implement three representative attitude estimation algorithms: the Quaternion Estimator (QUEST), the Multiplicative Extended Kalman Filter (MEKF), and a recent Globally Exponentially Stable Cascade Attitude Nonlinear Observer and 4) Analyze and compare the three algorithms in terms of computational resources efficiency and performance in various realistic simulation scenarios. Ultimately, this work must use the estimation algorithms to solve the problem of attitude estimation in conditions representative of the two missions, giving meaningful insight on the advantages, disadvantages, computational resources efficiency and performance of the three algorithms, providing the project with a grounded analysis that can be used for decision making in terms of the ADCS system design.

1.2. Literature Review

Some of the earliest solutions to the attitude estimation problem are deterministic methods that provide algebraic solutions based on two or more measurements taken at the same time. Among these solutions, the TRIAD algorithm was the first, but it was only able to use two measurements. Fighting this limitation, Grace Wahba formulated a general criterion for attitude determination using two or more measurements [16], that led to several alternative solutions [11, 10, 15] such as Davenport's q-method, QUEST algorithm and SVD algorithm.

Other solutions try to find the best estimate of the true attitude using dynamical models and measurements, both corrupted by noise and uncertainties. From these approaches, the ones based on Kalman filtering [6], may be highlighted. Since the models involved are nonlinear, the Extended Kalman Filter (EKF) is used to address nonlinear estimation problems [7]. The EKF earned then a reputation, becoming the most used method to determine the attitude of a spacecraft. EKF solutions come in several forms, such as the Additive EKF (AEKF) or the Multiplicative EKF (MEKF) [8].

However being a very powerful estimation technique, the EKF estimators do not give guarantees of optimality, stability or convergence and other nonlinear approaches rose in the attempt to overcome poor performance or even divergence arising from the linearization implicit in the EKF. Some of those alternatives are well documented in [3]. Unscented filters [5], particle filters, the two-step optimal estimator [4], predictive and adaptive approaches, and nonlinear observers should be highlighted.

2. Theoretical Background

2.1. Attitude Representations

The spacecraft attitude is the orientation of the spacecraft body frame $\mathcal{B}$, with respect to an inertial reference frame $\mathcal{I}$. This orientation may be represented or parameterized in various forms. Among the most representatives are the rotation matrix belonging to the Special Orthogonal *group* SO(3), the quaternion, adopting the convention of references [9, 10] and the Euler Angles. The asymmetric Euler angle sequence 3-2-1, was chosen to be the Euler angles sequence of reference, following the notation present in [10].

2.2. Reference Frames

A frame is specified by its origin and the orientation of its coordinate axes. In this work, the approximately inertial Earth-Centered Inertial Frame (ECI), denoted by $\mathcal{I} = \{\mathfrak{i}_1, \mathfrak{i}_2, \mathfrak{i}_3\}$ is used as the inertial reference frame. It has its origin at the center of mass of the Earth and the axes aligned with the mean North Pole and mean vernal equinox at some epoch. The spacecraft body frame considered, denoted by $\mathcal{B} = \{\mathfrak{b}_1, \mathfrak{b}_2, \mathfrak{b}_3\}$, has its origin at the center of mass of the satellite and its axes rotating with the spacecraft. The $\mathfrak{b}_3$ axis is aligned in the direction of the main scientific payload, $\mathfrak{b}_1$ is aligned with the normal to the bottom plate of the satellite, and $\mathfrak{b}_2$ completes the right-handed system.

2.3. Attitude Kinematics and Dynamics

Assuming the attitude is parameterized by a quaternion, the following equations are enough to model the rotational motion of the satellite rigid body:

$$\dot{\boldsymbol{H}}_{\mathcal{I}}^{c} = \boldsymbol{L}_{\mathcal{I}}^{c} \tag{1a}$$

$$\boldsymbol{H}_{\mathcal{B}}^{c} = \mathbf{A}(\mathbf{q}_{\mathcal{BI}})\boldsymbol{H}_{\mathcal{I}}^{c} \tag{1b}$$

$$\boldsymbol{\omega}_{\mathcal{B}}^{\mathcal{BI}} = (\boldsymbol{J}_{\mathcal{B}}^{c})^{-1}\boldsymbol{H}_{\mathcal{B}}^{c} \tag{1c}$$

$$\dot{\mathbf{q}}_{\mathcal{BI}} = \frac{1}{2}\boldsymbol{\omega}_{\mathcal{B}}^{\mathcal{BI}} \otimes \mathbf{q}_{\mathcal{BI}} \tag{1d}$$

where $\mathbf{q}_{\mathcal{BI}}$ is the quaternion that rotates from frame $\mathcal{I}$ to $\mathcal{B}$, $\mathbf{A}(\mathbf{q}_{\mathcal{BI}})$ is the rotation matrix formed from $\mathbf{q}_{\mathcal{BI}}$, $\boldsymbol{H}$ is the angular momentum, $\boldsymbol{J}$ is the moment of inertia tensor, $\boldsymbol{L}$ is the external net torque, $\boldsymbol{\omega}_{\mathcal{B}}^{\mathcal{BI}}$ is the angular velocity of frame $\mathcal{B}$ with respect to frame $\mathcal{I}$, mapped in frame $\mathcal{B}$, and $\otimes$ is the quaternion multiplication as defined in [10]. The external torques are composed by intentional control torques and by disturbance torques from different sources.

3. Attitude Determination Methods

This section documents the theory underlying the attitude determination methods that are the focus of this work.

3.1. Quaternion Estimator (QUEST)

The QUEST algorithm is a solution to a problem posed in 1965 by Grace Wahba [16]. Wahba's problem is to find the orthogonal matrix $\mathbf{A}$ with determinant $+1$ that minimizes the following loss function:

$$L(\mathbf{A}) = \frac{1}{2}\sum_{i=1}^{N} a_i||\mathbf{b}_i - \mathbf{A}\mathbf{r}_i||^2 \quad (2)$$

where $\mathbf{b}_i$ and $\mathbf{r}_i$ are respectively unitized measurements in the body and inertial frames and a_i are non-negative weights.

The loss function of equation 2 can be written in the quaternion form as:

$$L(\mathbf{A}(\mathbf{q})) = \lambda_0 - \mathbf{q}^T\mathbb{K}(\mathbb{B})\mathbf{q} \quad (3)$$

with:

$$\lambda_0 \equiv \sum_{i=1}^{N} a_i, \qquad \mathbb{B} \equiv \sum_{i=1}^{N} a_i\mathbf{b}_i\mathbf{r}_i^T, \quad (4a)$$

$$\mathbb{K}(\mathbb{B}) = \begin{bmatrix} \mathbb{S} - tr(\mathbb{B})\mathbf{I}_3 & \mathbb{z} \\ \mathbb{z}^T & tr(\mathbb{B}) \end{bmatrix} \quad (4b)$$

$$\mathbb{S} = \mathbb{B} + \mathbb{B}^T \ , \ \mathbb{z} = \begin{bmatrix} \mathbb{B}_{23} - \mathbb{B}_{32} \\ \mathbb{B}_{31} - \mathbb{B}_{13} \\ \mathbb{B}_{12} - \mathbb{B}_{21} \end{bmatrix} \quad (4c)$$

The minimization of $L(\mathbf{A}(\mathbf{q}))$ is achieved by finding the solution $\widehat{\mathbf{q}}$ of the characteristic-value problem:

$$\mathbb{K}\widehat{\mathbf{q}} = \lambda_{max}\widehat{\mathbf{q}} \quad (5)$$

where λ_{max} is the largest eigenvalue of $\mathbb{K}$. Thus the central part of the QUEST algorithm is the computation of λ_{max}. This is achieved by application of the Newton-Raphson method to the characteristic polynomial of $\mathbb{K}$, with initial estimate λ_0:

$$\Psi(\lambda) = det(\lambda\mathbf{I}_4 - \mathbb{K}) \quad (6)$$

being a single iteration generally sufficient. For QUEST, this polynomial has the form:

$$0 = [\lambda^2 - (tr(\mathbb{B}))^2 + \kappa][\lambda^2 - (tr(\mathbb{B}))^2 - ||\mathbb{z}||^2] - (\lambda - tr(\mathbb{B}))(\mathbb{z}^T\mathbb{S}\mathbb{z} + det\mathbb{S}) - \mathbb{z}^T\mathbb{S}^2\mathbb{z}$$

with $\kappa \equiv tr(adj(\mathbb{S}))$, and $adj(\,)$ the adjoint matrix.

3.2. Multiplicative Extended Kalman Filter (MEKF)

One traditional MEKF implementation onboard of satellites, and the one used in this work, is the 6-state EKF presented in [10], that estimates the current attitude and gyroscope biases simultaneously. The MEKF is formulated in terms of the error estimation, following the normal approach of EKF. MEKF uses the quaternion nonsingular representation for a reference attitude, and a three component representation for the deviations from this reference, representing the true quaternion as the product of an error quaternion $\boldsymbol{\delta}\mathbf{q}$ and the estimate $\widehat{\mathbf{q}}$:

$$\mathbf{q} = \boldsymbol{\delta}\mathbf{q}(\boldsymbol{\delta\vartheta}) \otimes \widehat{\mathbf{q}} \quad (7)$$

where $\boldsymbol{\delta\vartheta}$ is an attitude parameterization called rotation vector useful for representing small attitudes.

The 7-component global state vector $\mathbf{x}$ and the 6-component state error vector $\boldsymbol{\Delta}\mathbf{x}$ are:

$$\mathbf{x} \equiv \begin{bmatrix} \mathbf{q} \\ \boldsymbol{\beta} \end{bmatrix} \quad \boldsymbol{\Delta}\mathbf{x} \equiv \begin{bmatrix} \boldsymbol{\delta\vartheta} \\ \boldsymbol{\Delta\beta} \end{bmatrix} \quad (8)$$

where $\boldsymbol{\beta}$ is the gyro bias and $\boldsymbol{\Delta\beta}$ the bias error defined as $\boldsymbol{\Delta\beta} \equiv \boldsymbol{\beta} - \widehat{\boldsymbol{\beta}}$.

The continuous-time linearized MEKF error dynamic model and linearized error discrete measurement model are given by:

$$\Delta\dot{\mathbf{x}}(t) = \mathbf{F}(t)\Delta\mathbf{x}(t) + \mathbf{G}(t)\mathbf{w}(t) \quad (9a)$$

$$\boldsymbol{\upsilon}_k = \mathbf{H}_k\Delta\mathbf{x}_k + \mathbf{v}_k \quad (9b)$$

where $_k$ represents a quantity at time k, $\boldsymbol{\upsilon}_k = \mathbf{y}_k - \widehat{\mathbf{y}}_k$ is a measurement residual, $\mathbf{w}(t) \sim N(0, \mathbf{Q}(t))$ is a process noise vector, $\mathbf{v}_k \sim N(0, \mathbf{R}_k)$ is a measurement noise vector and:

$$\mathbf{F}(t) = \begin{bmatrix} -\left[\widehat{\boldsymbol{\omega}}(t)\times\right] & -\mathbf{I}_3 \\ \mathbf{0}_{3\times3} & \mathbf{0}_{3\times3} \end{bmatrix}, \mathbf{G}(t) = \begin{bmatrix} -\mathbf{I}_3 & \mathbf{0}_{3\times3} \\ \mathbf{0}_{3\times3} & \mathbf{I}_3 \end{bmatrix} \quad (10)$$

$$\mathbf{Q}(t) = \begin{bmatrix} \boldsymbol{\sigma}_{\boldsymbol{v}}^2\mathbf{I}_3 & \mathbf{0}_{3\times3} \\ \mathbf{0}_{3\times3} & \boldsymbol{\sigma}_{\boldsymbol{u}}^2\mathbf{I}_3 \end{bmatrix}, \mathbf{H}_k(\widehat{\mathbf{x}}_k^-) = \begin{bmatrix} \left[\widehat{\mathbf{b}}_1^- \times\right] & \mathbf{0}_{3\times3} \\ \left[\widehat{\mathbf{b}}_2^- \times\right] & \mathbf{0}_{3\times3} \\ \vdots & \vdots \\ \left[\widehat{\mathbf{b}}_N^- \times\right] & \mathbf{0}_{3\times3} \end{bmatrix}_{t_k} \quad (11)$$

where $\widehat{\boldsymbol{\omega}}$ is the estimated angular rate, and a continuous time model for the angular rate is provided by the gyro:

$$\boldsymbol{\omega}_m(t) = \boldsymbol{\omega}(t) + \boldsymbol{\beta}(t) + \boldsymbol{\eta}_v(t) \quad (12a)$$

$$\dot{\boldsymbol{\beta}}(t) = \boldsymbol{\eta}_u(t) \quad (12b)$$

where $\boldsymbol{\omega}(t)$ is the true rate, $\boldsymbol{\omega}_m(t)$ is the measured rate, $\boldsymbol{\beta}(t)$ is the true bias or drift, and $\boldsymbol{\eta}_v(t)$ and $\boldsymbol{\eta}_u(t)$ are independent zero-mean Gaussian white-noise processes, with standard deviations $\boldsymbol{\sigma}_{\boldsymbol{v}}$ and $\boldsymbol{\sigma}_{\boldsymbol{u}}$, respectively.

The MEKF implementation proceeds by iteration of three steps: 1) the measurement update, following from Kalman filter and EKF formulation; 2) the reset , that moves the updated information from the error state $\boldsymbol{\Delta}\mathbf{x}^+$ to the global state $\mathbf{x}^-$ and resets the components of the error state to zero, according to:

$$\widehat{\mathbf{q}}^+ = \boldsymbol{\delta}\mathbf{q}(\boldsymbol{\delta}\widehat{\boldsymbol{\vartheta}}^+) \otimes \widehat{\mathbf{q}}^- \quad (13a)$$

$$\widehat{\boldsymbol{\beta}}^+ = \widehat{\boldsymbol{\beta}}^- + \boldsymbol{\Delta}\widehat{\boldsymbol{\beta}}^+ \quad (13b)$$

and 3) the propagation step. In the propagation step, there is only need to propagate the state $\widehat{\mathbf{x}}$, but not the errors, which are null. This is done resorting to equation:

$$\dot{\widehat{\mathbf{q}}} = \frac{1}{2}\mathbf{\Omega}(\widehat{\boldsymbol{\omega}})\widehat{\mathbf{q}} \tag{14}$$

with:

$$\mathbf{\Omega}(\widehat{\boldsymbol{\omega}}) \equiv \begin{bmatrix} -\left[\widehat{\boldsymbol{\omega}}\times\right] & \widehat{\boldsymbol{\omega}} \\ -\widehat{\boldsymbol{\omega}}^T & 0 \end{bmatrix} \tag{15}$$

The covariance propagation is performed using the typical Kalman formulation.

An MEKF variation of this filter is used based on an algorithm developed by Murrell [13], where each vector observation is processed at a time, reducing the computationally complexity of the algorithm.

3.3. GES Cascade Observers

On [1], the authors presented the design, analysis, and performance evaluation of a novel cascade observer for attitude and bias estimation. The observer presented in that reference has globally exponentially stable (GES) error dynamics, is computationally efficient, is based on the angular motion kinematics, which are exact, builds on well-established Lyapunov results, explicitly estimates rate gyro bias and copes well with slowly time-varying bias, and has a complementary structure, fusing low bandwidth vector observations with high bandwidth rate gyro measurements. That solution was implemented in this work.

In the design of this observer, a sensor-based approach is performed. The filter is designed directly in the space of the sensors, and afterwards, using filtered estimates of the observations, the attitude can be determined. As the filtering occurs prior to the determination of attitude, the rotation matrix may be used as the attitude parameterization, which is unique, without singularities, and where topological restrictions on $SO(3)$ for achieving global asymptotic stability no longer apply and unwinding phenomena does not occur [12]. The sensor measurements are included directly in the system dynamics, and the kinematics are propagated using the angular velocity provided by a gyroscope.

Considering the rotation matrix $\mathbf{A}(t) \in SO(3)$, from $\{\mathcal{B}\}$ to $\{\mathcal{I}\}$, the attitude kinematics are given by:

$$\dot{\mathbf{A}}(t) = \mathbf{A}(t)\mathbf{S}(\boldsymbol{\omega}(t)) \tag{16}$$

where $\boldsymbol{\omega}(t) \in \mathbb{R}^3$ is the angular velocity of $\{\mathcal{B}\}$, expressed in $\{\mathcal{B}\}$, and $\mathbf{S}(\mathbf{x})$ is the skew-symmetric matrix such that $\mathbf{S}(\mathbf{x})\mathbf{y} = \mathbf{x}\times\mathbf{y}$. Assuming that a vector observation measurement $\mathbf{b}_1 \in \mathbb{R}^3$ is available, in body frame coordinates, of a known constant vector quantity $\mathbf{r}_1 \in \mathbb{R}^3$ in inertial coordinates:

$$\mathbf{r}_1 = \mathbf{A}(t)\mathbf{b}_1(t) \tag{17}$$

then, its dynamics are:

$$\dot{\mathbf{b}}_1(t) = -\mathbf{S}(\boldsymbol{\omega}(t))\mathbf{b}_1(t) \tag{18}$$

Considering the gyro model with constant bias:

$$\boldsymbol{\omega}_m(t) = \boldsymbol{\omega}(t) + \boldsymbol{\beta}(t) \tag{19}$$

then, the system dynamics, extended for N vector observation measurements, may be written as:

$$\begin{cases} \dot{\mathbf{b}}_1(t) = -\mathbf{S}(\boldsymbol{\omega}_m(t))\mathbf{b}_1(t) - \mathbf{S}(\mathbf{b}_1(t))\boldsymbol{\beta}(t) \\ \vdots \\ \dot{\mathbf{b}}_N(t) = -\mathbf{S}(\boldsymbol{\omega}_m(t))\mathbf{b}_N(t) - \mathbf{S}(\mathbf{b}_N(t))\boldsymbol{\beta}(t) \\ \dot{\boldsymbol{\beta}}(t) = \mathbf{0} \end{cases} \tag{20}$$

Bias Observer

The following design is based on the assumption that there exist at least two non-collinear reference vectors, i.e., there exist i and j such that $\mathbf{r}_i \times \mathbf{r}_j \neq 0$ (from now on referred as Assumption 1). Assumption 1 is necessary for attitude estimation. Using the system dynamics of equation 20 the bias observer is given by:

$$\begin{cases} \dot{\widehat{\mathbf{b}}}_1(t) = -\mathbf{S}(\boldsymbol{\omega}_m(t))\widehat{\mathbf{b}}_1(t) - \mathbf{S}(\mathbf{b}_1(t))\widehat{\boldsymbol{\beta}}(t) + \alpha_1\tilde{\mathbf{b}}_1(t) \\ \vdots \\ \dot{\widehat{\mathbf{b}}}_N(t) = -\mathbf{S}(\boldsymbol{\omega}_m(t))\widehat{\mathbf{b}}_N(t) - \mathbf{S}(\mathbf{b}_N(t))\widehat{\boldsymbol{\beta}}(t) + \alpha_N\tilde{\mathbf{b}}_N(t) \\ \dot{\widehat{\boldsymbol{\beta}}}(t) = \sum_{i=1}^{N}\gamma_i\mathbf{S}(\mathbf{b}_i(t))\tilde{\mathbf{b}}_i(t) \end{cases} \tag{21}$$

where $i = 1, ..., N$, $\tilde{\mathbf{b}}_i(t) \equiv \mathbf{b}_i(t) - \widehat{\mathbf{b}}_i(t)$, are the errors of the vector observation estimates, and α_i, γ_i, are positive scalar constants. Under Assumption 1, the origin of this Bias Observer error dynamics is a GES equilibrium point. Proof for this statement may be found in Section 3.1 of [1].

Attitude Observer

The following design is made on the assumption that the matrix $\left[\mathbf{r}_1 \dots \mathbf{r}_N\right] \in \mathbb{R}^{3\times3N}$ has full rank (from now on referred as Assumption 2), which, given a set of reference vectors that satisfy Assumption 1, it is always possible: If $\mathbf{r}_i \in \mathbb{R}^3$ and $\mathbf{r}_j \in \mathbb{R}^3$ denote two non-collinear reference vectors, then, the set $\{\mathbf{r}_i, \mathbf{r}_j, \mathbf{r}_i \times \mathbf{r}_j\}$ satisfies Assumption 2.

Considering an alternative column representation of the rotation matrix $\mathbf{A}(t)$ given by:

$$\boldsymbol{\chi}_2(t) = \begin{bmatrix} \mathbf{z}_1(t) \\ \mathbf{z}_2(t) \\ \mathbf{z}_3(t) \end{bmatrix} \in \mathbb{R}^9, \quad \mathbf{A}(t) = \begin{bmatrix} \mathbf{z}_1^T(t) \\ \mathbf{z}_2^T(t) \\ \mathbf{z}_3^T(t) \end{bmatrix} \tag{22}$$

Under Assumption 2 and knowing the rate gyro bias, the following dynamics take place:

$$\dot{\boldsymbol{\chi}}_2(t) = -\mathbf{S}_3(\boldsymbol{\omega}_m(t) - \boldsymbol{\beta}(t))\boldsymbol{\chi}_2(t) \tag{23}$$

where:

$$\mathbf{S}_3(\mathbf{x}) \equiv diag(\mathbf{S}(\mathbf{x}), \mathbf{S}(\mathbf{x}), \mathbf{S}(\mathbf{x})) \in \mathbb{R}^{9\times9} \tag{24}$$

Using 17, the vector observations can be written as a function of $\boldsymbol{\chi}_2(t)$ by:

$$\mathbf{b}(t) = \mathbf{C}_2\boldsymbol{\chi}_2(t) \tag{25}$$

with:

$$\mathbf{C}_2 = \begin{bmatrix} r_{11} & 0 & 0 & r_{12} & 0 & 0 & r_{13} & 0 & 0 \\ 0 & r_{11} & 0 & 0 & r_{12} & 0 & 0 & r_{13} & 0 \\ 0 & 0 & r_{11} & 0 & 0 & r_{12} & 0 & 0 & r_{13} \\ & & & & \vdots & & & & \\ r_{N1} & 0 & 0 & r_{N2} & 0 & 0 & r_{N3} & 0 & 0 \\ 0 & r_{N1} & 0 & 0 & r_{N2} & 0 & 0 & r_{N3} & 0 \\ 0 & 0 & r_{N1} & 0 & 0 & r_{N2} & 0 & 0 & r_{N3} \end{bmatrix} \in \mathbb{R}^{3N\times 9} \tag{26}$$

The attitude observer can then be given by:

$$\dot{\widehat{\boldsymbol{\chi}}}_2(t) = -\mathbf{S}_3(\boldsymbol{\omega}_m(t) - \boldsymbol{\beta}(t))\widehat{\boldsymbol{\chi}}_2(t) + \mathbf{C}_2^T \mathtt{Q}^{-1}[\mathbf{b}(t) - \mathbf{C}_2\widehat{\boldsymbol{\chi}}_2(t)] \tag{27}$$

where $\mathtt{Q} = \mathtt{Q}^T \in \mathbb{R}^{3N\times 3N}$ is a positive definite matrix. With knowledge of the rate gyro bias and under Assumption 2, the origin of this attitude observer error dynamics is a GES equilibrium point. Proof for this statement may be found in section 3.2 of [1].

Cascade Observer

The cascade observer feeds the attitude observer with the bias estimate provided by the bias observer. The full cascade observer becomes:

$$\begin{cases} \dot{\widehat{\mathbf{b}}}_1(t) = -\mathbf{S}(\boldsymbol{\omega}_m(t))\widehat{\mathbf{b}}_1(t) - \mathbf{S}(\mathbf{b}_1(t))\widehat{\boldsymbol{\beta}}(t) + \alpha_1\tilde{\mathbf{b}}_1(t) \\ \vdots \\ \dot{\widehat{\mathbf{b}}}_N(t) = -\mathbf{S}(\boldsymbol{\omega}_m(t))\widehat{\mathbf{b}}_N(t) - \mathbf{S}(\mathbf{b}_N(t))\widehat{\boldsymbol{\beta}}(t) + \alpha_N\tilde{\mathbf{b}}_N(t) \\ \dot{\widehat{\boldsymbol{\beta}}}(t) = \sum_{i=1}^N \gamma_i \mathbf{S}(\mathbf{b}_i(t))\tilde{\mathbf{b}}_i(t) \\ \dot{\widehat{\boldsymbol{\chi}}}_2(t) = -\mathbf{S}_3(\boldsymbol{\omega}_m(t) - \widehat{\boldsymbol{\beta}}(t))\widehat{\boldsymbol{\chi}}_2(t) + \mathbf{C}_2^T\mathtt{Q}^{-1}[\widehat{\mathbf{b}}(t) - \mathbf{C}_2\widehat{\boldsymbol{\chi}}_2(t)] \end{cases} \tag{28}$$

where, for performance purposes, particularly in the presence of sensor noise, the vector estimate $\widehat{\mathbf{b}}(t)$ provided by the bias observer is used in feedback. The origin of this cascade observer error dynamics is a GES equilibrium point. Proof for this statement may be found in sections 3.3 and 3.4 of [1].

4. Implementation

The simulation environment developed aims at realistically describe the conditions felt by the spacecraft. It is composed of an environment model, that simulates the position of other celestial objects and disturbance effects on the acceleration and torque of the spacecraft, a dynamic model that simulates the effects of forces and torques on the nanosatellite, propagating its orbit and attitude, a suite of sensor models that calculate the sensors outputs, and, finally, the implementation of the estimation algorithms proposed.

The sensor suite assumed available onboard for purposes of attitude determination is composed by a rate gyroscope, a Sun sensor, a magnetometer and a star tracker. The sensor characteristics selected are those of the ST-16 star tracker from Sinclair Interplanetary, the RM3100 magnetometer from PNI Corp, the Fine Digital Sun Sensor from New Space systems and the LN-200S gyroscope from the Northrop Grumman. Sensors characteristics are presented in Table 1.

Sensor	Freq.	Noise Std. Dev.
Gyroscope	100 Hz	$\sigma_v = 1.18\times 10^{-2}\ {}^\circ/s$
		$\sigma_u = 2.78\times 10^{-4}\ {}^\circ/s$
Magnetometer	100 Hz	$\sigma_{mag} = 30nT$
Sun sensor	100 Hz	$\sigma_{ss} \approx 1.70\times 10^{-3}rad$
Star tracker	10 Hz	$\sigma_{star} = 3.59\times 10^{-4}rad$

Table 1: Sensor characteristics.

For simulation purposes, the QUEST algorithm, the MEKF and the GES Nonlinear Observers were implemented, operating at $10Hz$, $100Hz$ and $100Hz$, respectively. For discrete implementation, the dynamical system 28 was discretized using the first-order Euler method, with the right side of the system subject to sample-and-hold. Observer parameters were tuned to achieve a balance between estimation error and convergence. The parameters $\alpha_i = 1\,, i = 1, ..., N$, $\gamma_i = 0.016\,, i = 1, ..., N$ and $\mathtt{Q} = 0.03$ were used.

4.1. Computational Resources Efficiency Analysis

One way to quantify the computational complexity of an algorithm is to count FLOPs. The number of FLOP needed to run each of the three algorithms was analyzed and compared. Filter operation with the rates selected and with four available vector measurements, namely the Sun sensor measurement and the three star tracker measurements, was considered, reaching the values presented in Table 2.

	QUEST	MEKF	NL Observer
FLOPs	3010	296500	122900

Table 2: Required FLOPs for the three filters operation.

5. Results

The implemented algorithms were tested in the realistic environment created with different simulation case scenarios. Some characteristics are common: The satellite dynamics and kinematics are simulated in continuous-time, while the attitude determination methods are run in discrete-time; The solver used is the fixed-step eighth order Dormand-Prince method with a fixed time-step of $0.01\,s$; It is assumed that the satellite has been detumbled before the attitude estimation begins and no control torque is applied during the simulations; The true attitude is assumed to be the one generated by the simulator, which is considered reality in the simulation. Two different orbits were used to perform the simulations. Orbit 1 was selected as a Geostationary Transfer Orbit (GTO) and orbit 2 is a typical Low-Earth Orbit. Implications of these two orbits essentially differ on the acceleration and torque perturbations present, and on the availability of the magnetometer sensor, which is not available in orbit 1. All other sensors are available in both orbits.

Case 1

Case 1 aimed at comparing the three attitude determination algorithms implemented, with all the sensors available. The true initial attitude was defined as the identity quaternion $\mathbf{q}_0 = [0,\, 0,\, 0,\, 1]^T$ and the initial bias was $\boldsymbol{\beta}_0 = \frac{\pi}{180}[-0.02,\, 0.03,\, -0.01]^T rad\, s^{-1}$. The angular rate followed $\boldsymbol{\omega} = \frac{\pi}{180}[0.1\,\cos(\frac{2\pi}{200}t),\, 0.15\,\cos(\frac{2\pi}{180}t),\, 0.05\,\cos(\frac{2\pi}{200}t)]^T$ rad/s. The MEKF and NL observer were initialized with a considerable attitude and bias estimation error. The initial attitude estimate was $\widehat{\mathbf{q}}_0 = [6.0692 \times 10^{-02}, 6.9371 \times 10^{-01}, 6.0692 \times 10^{-02}, 7.1512 \times 10^{-01}]^T$, corresponding to an initial attitude estimation error in terms of Euler angles of $\delta\phi = 80°$, $\delta\theta = 80°$ and $\delta\psi = 80°$. The initial bias estimate was $\widehat{\boldsymbol{\beta}}_0 = [0,\, 0,\, 0]^T\ rad\, s^{-1}$, corresponding to a initial bias estimation error of $||\Delta\widehat{\boldsymbol{\beta}}_0|| = 134.70\,°\,h^{-1}$, in magnitude. The initial covariance matrix for the MEKF was defined as $\mathbf{P}_0 = diag(100, 100, 100, 10, 10, 10)$, reflecting the uncertainty of the initial estimates. The NL observer estimates for the measurements were initialized as zero, and the observer parameters were tuned as stated before.

The three algorithms ran in parallel, in a simulation of $3600s$. The detailed evolution of the angular estimation error, represented as Euler angles, after the initial transient faded out, for orbit 1, is presented in figure 1, and the root-mean-square errors, for the simulation of the two orbits, are available in Table 3.

The initial convergence of the angular estimation error, for the simulation in orbit 1 is represented in figure 2, and the detailed evolution of the bias estimation error can be seen in figure 3.

Case 2

Case 2 aimed at studying the estimation performance when the star tracker has a fault. The same initial simulation conditions of Case 1 were used. The star tracker was assumed to enter into fault at time $1100s$. After the complete failure of the sensor, in the case of simulations in orbit 1, just the Sun sensor was left available, while in the case of simulations in orbit 2, both the Sun sensor and the magnetometer were available. When just one measurement is available, the QUEST and NL Observer

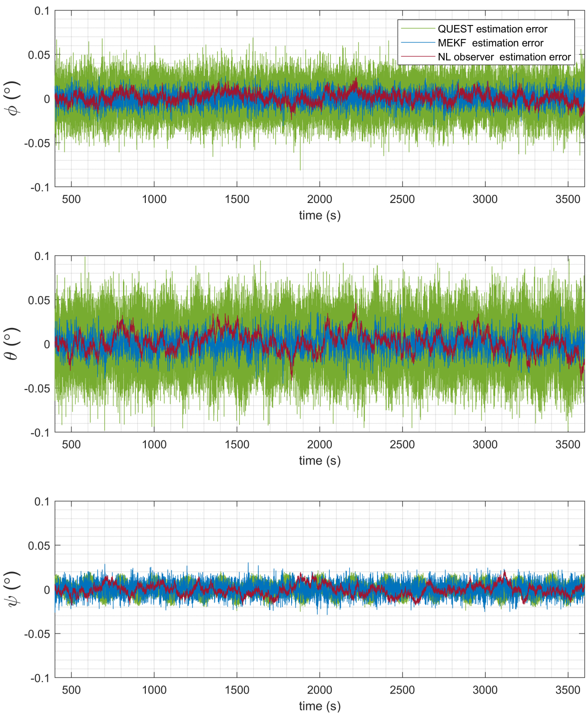

Figure 1: Detailed evolution of the angular estimation error for simulation case 1, orbit 1.

	Orbit 1		
	QUEST	MEKF	NL observer
ϕ_{RMS} (°)	1.7214×10^{-2}	7.0025×10^{-3}	6.2568×10^{-3}
θ_{RMS} (°)	2.5538×10^{-2}	1.0120×10^{-2}	1.1909×10^{-2}
ψ_{RMS} (°)	5.4279×10^{-3}	6.8745×10^{-3}	6.2647×10^{-3}
	Orbit 2		
	QUEST	MEKF	NL observer
ϕ_{RMS} (°)	1.6992×10^{-2}	1.0059×10^{-2}	5.9629×10^{-3}
θ_{RMS} (°)	2.3371×10^{-2}	1.9754×10^{-2}	1.1167×10^{-2}
ψ_{RMS} (°)	9.6787×10^{-3}	9.0957×10^{-3}	5.9824×10^{-3}

Table 3: Root Mean Square of the angular estimation error for the QUEST, the MEKF and the NL observer for simulation case 1 in the interval ($400s$; $3600s$).

cannot run, hence, an open loop propagation takes place starting from the last estimate of each algorithm. While the propagation for QUEST was done directly using the angular rate provided by the gyro, for the NL observer, the same angular rate was corrected using the last bias estimate of the filter. The three algorithms ran in parallel. The detailed evolution of the angular estimation error, represented as Euler angles, with the star tracker fault happening after the initial transient faded out, for the two orbits, is presented in figure 4, and the respective root-mean-square errors are available in Table 4.

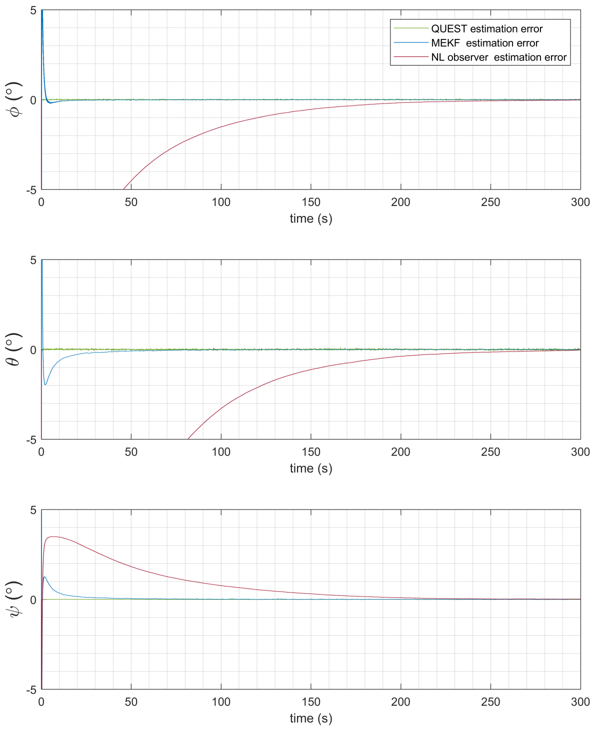

Figure 2: Initial convergence of the angular estimation error for simulation case 1, orbit 1.

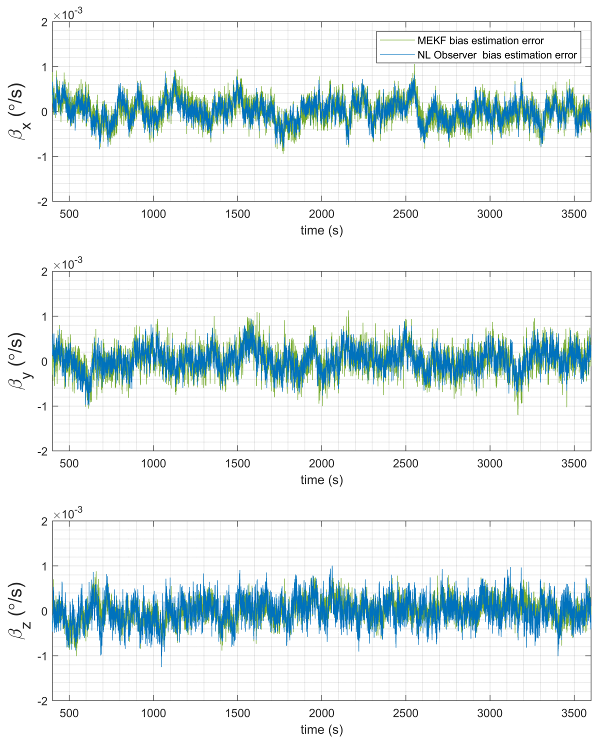

Figure 3: Detailed evolution of the bias estimation error for simulation case 1, orbit 1

Case 3

Case 3 aimed at studying the estimation performance when only the star tracker was available. The same initial conditions of Case 1 were used. A simulation in orbit 2 was performed where at $750s$ the Sun sensor and the magnetometer suffered a fault. From $750s$ to $3600s$, the three estimation filters ran only with the measurements provided by the star tracker. The detailed evolution of the angular estimation error after the initial transient faded

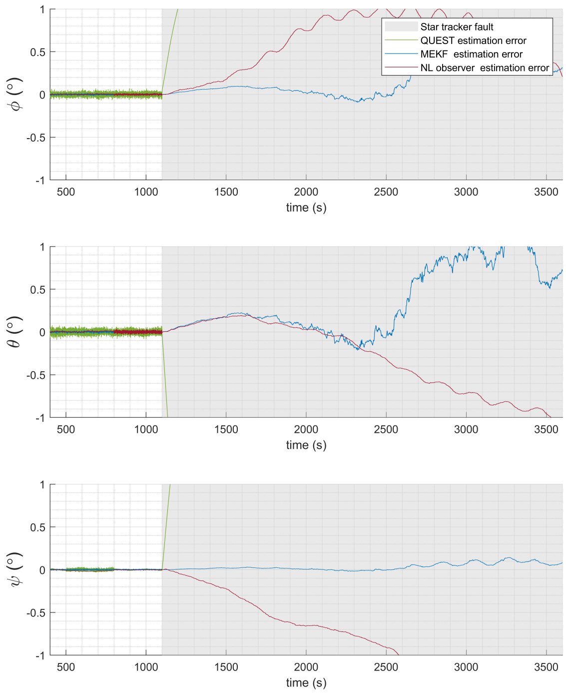

(a) Orbit 1

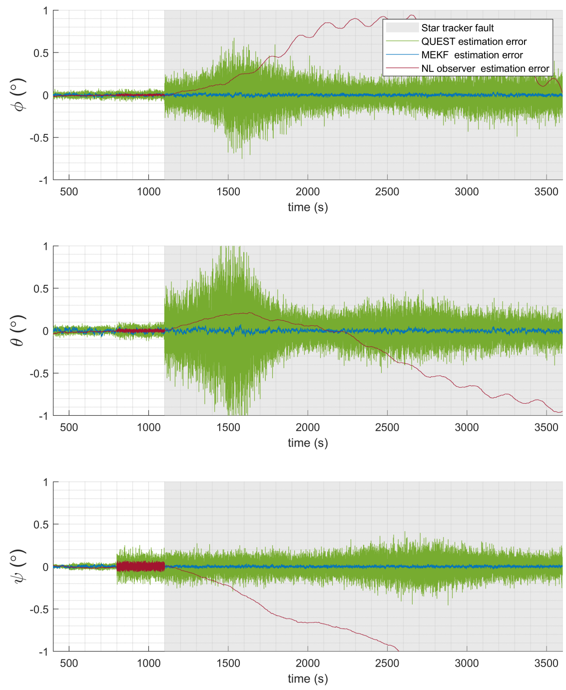

(b) Orbit 2

Figure 4: Detailed evolution of the angular estimation error for simulation case 2.

	Orbit 1		
	QUEST	MEKF	NL observer
ϕ_{RMS} (°)	3.4094×10^{1}	2.3245×10^{-1}	6.9455×10^{-1}
θ_{RMS} (°)	3.1325×10^{1}	5.3866×10^{-1}	5.0615×10^{-1}
ψ_{RMS} (°)	4.2578×10^{1}	5.1819×10^{-2}	9.2886×10^{-1}
	Orbit 2		
	QUEST	MEKF	NL observer
ϕ_{RMS} (°)	1.2279×10^{-1}	1.0339×10^{-2}	6.0389×10^{-1}
θ_{RMS} (°)	1.8045×10^{-1}	1.6615×10^{-2}	4.6671×10^{-1}
ψ_{RMS} (°)	8.7629×10^{-2}	8.4730×10^{-3}	9.4055×10^{-1}

Table 4: Root Mean Square of the angular estimation error for the QUEST, the MEKF and the NL observer for simulation case 2 in the interval ($1100s$; $3600s$).

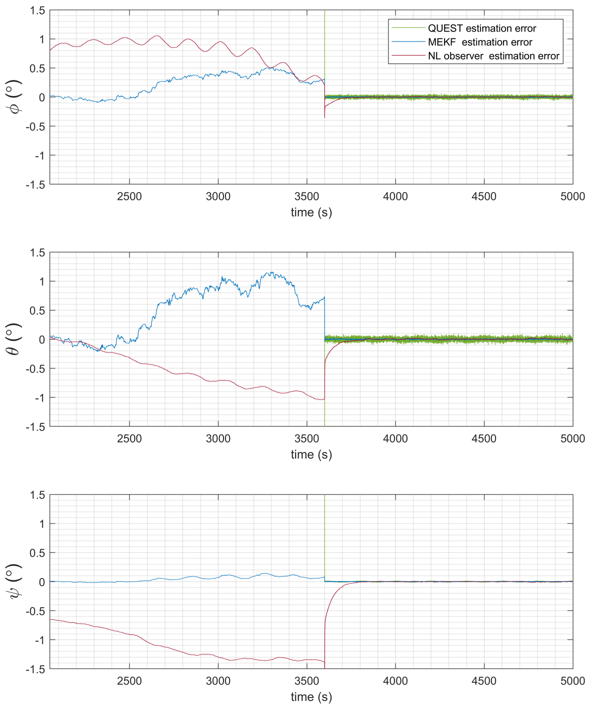

Figure 5: Detailed evolution of the angular estimation error for simulation case 4 with sensors reacquisition at $3600s$.

out was analyzed, and the respective root-mean-square errors are available in Table 5.

	QUEST	MEKF	NL observer
ϕ_{RMS} (°)	1.7251×10^{-2}	9.5974×10^{-3}	4.9036×10^{-3}
θ_{RMS} (°)	2.3712×10^{-2}	9.1414×10^{-3}	8.4132×10^{-3}
ψ_{RMS} (°)	9.6778×10^{-3}	5.7051×10^{-3}	7.4242×10^{-3}

Table 5: Root Mean Square of the angular estimation error for the QUEST, the MEKF and the NL observer for simulation case 3 in the interval ($750s$; $3600s$).

Case 4

Case 4 aimed at studying how the 3 filters responded in a situation of re-acquisition of sensors after a drift due to faults. The end of the simulation case 2, orbit 1, is a good example of a situation where a drift leads to considerable angular estimation errors, and was used as a starting point for simulation in case 4. After $3600s$, all the attitude sensors became available again. The three algorithms ran in parallel and the evolution of the angular estimation error, represented as Euler angles is presented in figure 5.

5.1. Discussion

Case 1

The analysis of results for Case 1 may start with the analysis of the initial transients for attitude and bias estimation. The QUEST algorithm, owing to its characteristics, does not have a transient period, achieving steady state performance from time $0s$. The MEKF achieves steady state for the three Euler angles before time $50s$. The NL observer has shown to be the algorithm with the biggest transient, needing $300s$ to achieve its steady state performance. Contrary to what happens in terms of attitude convergence, the NL observer bias estimation shows to converge to zero, in less than $100s$, which is faster than the MEKF bias estimation, which requires at least $200s$ to reach the same values. It is important to note that Case 1 simulates extreme conditions in terms of initial angular and bias estimation errors, which do not affect the QUEST estimates but have impact in the transient period for the MEKF and NL observer. A different tuning for the initial covariance, and for the observer parameters may translate in faster transients for the two algorithms. However, even with extreme conditions, the convergence times presented should not implicate any disadvantages in terms of a real application, and less initial error should translate into smaller transient periods.

The nominal mode or steady-state performance for the 3 algorithms can be analyzed by inspecting the detailed evolution of angular and bias estimation errors in figures 1 and 3, respectively. The behavior of the detailed evolution of the angular estimation error is similar for the simulation in orbit 1 or orbit 2, for the three algorithms, which indicates that the presence of the magnetometer, when all the other sensors are available, does not reflect in a better attitude estimation accuracy for the QUEST and MEKF. Overall, the QUEST algorithm has the biggest estimation error, followed by the MEKF and NL Observer that have approximately the same performance. In terms of the analysis of the bias estimation error evolution, the performance of the MEKF and the NL Observer is similar.

Case 2

The analysis of figure 4 and Table 4 leads to very different analysis for the two orbits, given the sensors left available in the two cases, which were the Sun sensor in the case of orbit 1 and the magnetometer and Sun sensor in the case of orbit 2. In the case of orbit 1, after the star tracker failure, the QUEST drifts very fast translating into a maximum root-mean-square error of $4.2578 \times 10^{1\circ}$. The NL observer, on the other hand, minimizes the drift effect for a longer period, but eventually reaches fairly high values of error when in comparison of those obtained in nominal mode. The MEKF shows to be robust in this situation, showing to be the one that looses estimation accuracy more slowly, and being able to keep the lower estimation error with only one measurement. In the case of orbit 2, both the QUEST and MEKF are able to continue running with the Sun sensor and magnetometer measurements, but the NL Observer is in the same situation as in orbit 1. After the star tracker failure, the angular error estimate for the QUEST shows to increase, with a root-mean-square error one order of magnitude higher. In the case of the MEKF, the angular estimation error increases in comparison with Case 1, but a good following is still achieved.

This case made evident some of the flaws or weaknesses of the three algorithms compared. It showed that QUEST is highly dependent on the availability of two vector measurements and not robust in practice, due to the lack of bias estimates. Additionally, without the star tracker, the increased angular estimation error evidenced reflects the QUEST highly dependence on the accuracy of the measurements used. It showed that the NL observer is able to mitigate the propagation errors in the case of lack of measurements but if this propagation is done for a long period, it will eventually drift to higher errors. Finally,the MEKF has shown to be the more robust of the 3 algorithms. Even with just one measurement, the filter showed to be the one minimizing the errors, and with the Sun sensor and magnetometer available, showed to be able to raise the importance of the rate gyro measurements when compared with the noisy Sun sensor and magnetometer.

Case 3

Case 3 analysis showed that the QUEST performance remained the same even only with the star tracker available, which was an expected result as the star tracker measurements are much more weighted in the QUEST algorithm than those coming from the Sun sensor and magnetometer. When it comes to the MEKF and NL Observer, a slightly better performance can be noticed, with less angular error variations, as can be deduced by comparing the root-mean-square errors in Table 5, with those of Table 3. The results obtained indicate that combining a magnetometer and Sun sensor with a star tracker does not necessarily give improved estimate accuracy, with the greater part of the accuracy coming from the star tracker. In fact, the bigger value of noise in the Sun sensor and magnetometer measurements can introduce variations in the estimates of the MEKF and NL Observer. That could be taken into account in future tuning of parameters, lowering the importance given to these two sensors in those processes.

Case 4

Case 4 has the importance of showing how these algorithms respond to a re-acquisition of sensors that were not working properly due to eclipses or faults. At time $3600s$, figure 5 points a considerable angular error estimation of more than 1° for some Euler angles. After the sensors re-acquisition, the QUEST convergence is immediate, as already was illustrated in the transient analysis in Case 1. The MEKF also shows an almost immediate convergence to values close to 0. On the other hand, the slower transients seen for the NL Observer in Case 1, are also visible in this analysis, where $200s$ are needed for the NL Observer angular estimate to converge again to values close to 0. This simulation appeals once more to the convergence characteristics of the three methods, where it is illustrated that even after a long drift due to unavailability of measurements, the nominal working mode can be retaken if the sensors start working again.

6. Conclusions

The deterministic method studied, QUEST, was the least computationally complex algorithm employed, requiring approximately 40 times less FLOPs than required by the NL Observer, the second least complex. The chosen rate at which the QUEST algorithm ran, ten times lower than the one of the NL Observer, contributed to the less computational resources usage, but evidence was shown that with the same rate, QUEST would still be the least computationally complex algorithm. A steady state performance in terms of angular estimation similar to the other two algorithms was achieved by QUEST, when all sensors were available. However, the accuracy obtained has shown to be highly dependent on the quality of the sensors measurements, and their availability, showing serious limitations in terms of robustness when the sensors suffer failures. Additionally, the lack of estimation of other quantities such as gyro biases is a negative point for this kind of methods, that ultimately translates into a serious practical disadvantage.

The MEKF, on the other hand, showed to be a very robust solution, dealing favorably with sensor faults. Its steady state performance in terms of angular estimation has revealed to be the best, in pair with the results for the NL Observer. However, its computational complexity has shown to be the greatest of the three algorithms requiring more than the double of FLOPs than the NL Observer. The MEKF is also the algorithm with the most complex formulation, without proofs of convergence, and with the need to define initial estimates that can negatively impact its performance. Its ability to also estimate gyro biases proved extremely important as the gyro measurements could be calibrated.

The Nonlinear observer offered a steady state performance approximately the same as the one provided by the MEKF. It also required less than half of the FLOPs when compared to the MEKF, was more easily formulated and implemented, and had a set of parameters that could be more intuitively tuned depending on the constraints. It has shown, however, to be less robust than the MEKF, due to its inability to use the magnetometer, but still with a moderate response to faults, and the ability to calibrate the gyroscope measurements. Overall, it has shown to be an attractive solution in comparison with the MEKF due to its proof of globally exponentially stability.

To finalize, the selection of one of these three algorithms for the implementation into the ADCS of a NANOSTAR mission will always be a trade-off between computer and implementation complexity, the importance of robustness, and the steady state accuracy needed.

Acknowledgements

The author would like to thank Professor Paulo Oliveira for his guidance, insightful discussions and valuable input, providing all the necessary facilities and equipment for this research.

References

[1] P. Batista, C. Silvestre, and P. Oliveira. Globally exponentially stable cascade observers for attitude estimation. *Control Engineering Practice*, 20(2):148–155, feb 2012.

[2] J. Bouwmeester and J. Guo. Survey of worldwide pico- and nanosatellite missions, distributions and subsystem technology. *Acta Astronautica*, 67(7-8):854–862, oct 2010.

[3] J. L. Crassidis, F. L. Markley, and Y. Cheng. Survey of Nonlinear Attitude Estimation Methods. *Journal of Guidance, Control, and Dynamics*, 30(1):12–28, jan 2007.

[4] G. T. Haupt, N. J. Kasdin, G. M. Keiser, and B. W. Parkinson. Optimal recursive iterative algorithm for discrete nonlinear least-squares estimation. *Journal of Guidance, Control, and Dynamics*, 19(3):643–649, may 1996.

[5] S. Julier, J. Uhlmann, and H. Durrant-Whyte. A new method for the nonlinear transformation of means and covariances in filters and estimators. *IEEE Transactions on Automatic Control*, 45(3):477–482, mar 2000.

[6] R. E. Kalman. A New Approach to Linear Filtering and Prediction Problems. *Journal of Basic Engineering*, 82(1):35, 1960.

[7] E. J. Lefferts, F. L. Markley, and M. D. Shuster. Kalman filtering for Spacecraft Attitude Estimation. In *20th Aerospace Sciences Meeting*, Reston, Virigina, jan 1982. American Institute of Aeronautics and Astronautics.

[8] F. L. Markley. Multiplicative vs. Additive Filtering for Spacecraft Attitude Determination. page 8, 2003.

[9] F. L. Markley, J. Crassidis, and Y. Cheng. Nonlinear Attitude Filtering Methods. In *AIAA Guidance, Navigation, and Control Conference and Exhibit*, Reston, Virigina, aug 2005. American Institute of Aeronautics and Astronautics.

[10] F. L. Markley and J. L. Crassidis. *Fundamentals of Spacecraft Attitude Determination and Control*. 2014.

[11] F. L. Markley and D. Mortari. Quaternion Attitude Estimation Using Vector Observations. *Journal of the Astronautical Sciences*, 48, 2000.

[12] P. T. Martins Batista. *Sensor-based Navigation and Control of Autonomous Vehicles*. PhD thesis, Instituto Superior Técnico, Universidade de Lisboa, 2010.

[13] J. W. Murrell. Precision Attitude Determination for Multimission Spacecraft. In *Guidance and Control Conference*, Reston, Virigina, aug 1978. American Institute of Aeronautics and Astronautics.

[14] NANOSTAR. The Project, 2018.

[15] M. D. Shuster and S. D. OH. Three-axis attitude determination from vector observations. *Journal of Guidance and Control*, 4(1):70–77, jan 1981.

[16] G. Wahba. A Least Squares Estimate of Satellite Attitude (Grace Wahba). *SIAM Review*, 8(3):384–386, jul 1966.